

# Design Optimization Methodology of Submarine Using Multilevel Numerical CFD Models

**Barhm Mohamad**

Erbil Polytechnic University  
Koya Technical Institute  
Department of Petroleum Technology  
44001 Erbil  
Iraq

**Salah Amroune**

Faculty of Technology University of M'sila  
Laboratory of Materials and Mechanics of  
Structures (LMMS)  
PO. Box. 166 Ichebilila 28000 M'sila  
Algeria

**Rached Miri**

University of Gafsa  
Faculty of Sciences  
Research Lab Technology Energy and  
Innovative Materials  
Tunisia

**Abdellah Benchekkour**

Tahri Mohammed University  
ENERGARID Laboratory  
P.O. Box 417, Bechar, 08000  
Algeria

**Karlen Galoyan**

Moscow Aviation Institute(National  
Research University)  
Department of Aircraft Aerodynamics  
125993 Moscow  
Russia

*This study explores the hydrodynamic and aerodynamic performance of a submarine and an airfoil under various angles of attack (AoA) using advanced computational fluid dynamics (CFD) simulations. The incompressible Reynolds Averaged Navier-Stokes (RANS) equations were solved using ANSYS, leveraging its segregated flow solver and adjoint optimization capabilities to automate the creation and meshing of computational domains. By analyzing velocity and pressure distributions across coarse and fine mesh resolutions, the research highlights the superior accuracy of fine meshes in capturing complex flow phenomena, such as flow separation, wake behavior, and velocity gradients. Submarine simulations with control surfaces revealed distinct symmetries and nearly zero maneuvering coefficients for specific configurations, filling gaps in the existing literature on fully appended geometries. Optimization efforts led to an enhanced design with improved aerodynamic efficiency, achieving reduced drag and stabilized flow, as validated by consistent performance at AoAs of 0°, 20°, and 80°. This work demonstrates the importance of fine mesh resolution, automated workflows, and adjoint solvers in accelerating the iterative design process and optimizing marine and aerodynamic structures for real-world applications. These findings highlight the significant influence of high attack angles on the submarine's vertical plane flow. Such insights offer a mechanical foundation for analyzing nonlinear motion phenomena during submarine surfacing.*

**Keywords:** Computational fluid dynamics, angle of attack, maneuvering technique, Complex design methodologies, hydrodynamic forces.

## 1. INTRODUCTION

The utilization of Computational Fluid Dynamics (CFD) as a means to replicate a standard set of hydrodynamic tests presents an appealing prospect. It holds the potential to be integrated into the design cycle earlier than traditional model testing, thereby mitigating some of the uncertainties inherent in established early design practices. Moreover, when properly calibrated, this tool serves as a valuable complement to model testing. By judiciously incorporating such a tool, the necessity for extensive model testing can be substantially reduced. The equations governing the motion of a maneuvering submarine consist of three equations for the force components (X, Y, Z) relative to the body-fixed axes (x ahead, y starboard, z down), and three equations for the moments (K, M, N) about these axes. It is conventional to express these equations in non-dimensional form.

Thus, the non-dimensional force  $\dot{X} = \frac{X}{0.5\rho UL^2}$  and the

non-dimensional moment  $\dot{K} = \frac{K}{0.5\rho UL^3}$  The effects of

various stimuli on the forces and moments are quantified by the maneuvering coefficients. For example, the coefficient representing the response of the sway force to a velocity perturbation in the y direction is

denoted as  $\dot{Y}_v = \frac{d\dot{Y}}{dv}$ . The determination of these mane-

uvering coefficients in the laboratory typically involves conducting a series of captive test sequences. Each sequence is arranged such that, for every sequence, only a restricted set of coefficients needs to be considered, while the rest can be neglected [1]. Mozaffari et al. (2022) conducted research focused on generating meshes with optimal resolution for hybrid RANS/LES simulations of high Reynolds number flows featuring complex physical phenomena and geometries. They highlighted the importance of automatic mesh generation using adaptive refinement. However, they noted that turbulence models' behavior depends on local grid size, meaning that mesh changes due to adaptive refinement could impact turbulence production and destruction. To address this, they proposed grid adaptation with refinement criteria based on time-averaged quantities. By averaging over the instantaneous flow field and refinement criterion, they simulated turbulent flow behind a backward-facing step using a Detached Eddy Simulation (DES) type turbulence model. Their findings revealed that compared to grid adaptation based on instantaneous solutions, this approach reduced computational cost, improved solution accuracy, and

Received: January 2025, Accepted: April 2025

Correspondence to: Dr Barhm Mohamad  
Department of Petroleum Technology, Koya Technical  
Institute, Erbil Polytechnic University, 44001 Erbil, Iraq  
E-mail: barhm.mohamad@epu.edu.iq

doi: 10.5937/fme2502280B

© Faculty of Mechanical Engineering, Belgrade. Allrights reserved

FME Transactions (2025) 53, 280-288 280

yielded an adapted mesh with a generally static topology aligned with main flow features. They further validated this refinement process through realistic test cases involving a ship and a hybrid delta wing, demonstrating the viability of average-based adaptation for automatic meshing in hybrid RANS/LES simulations of complex flows.

Parnaudeau et al. (2008) contribute to understanding the flow over a circular cylinder at a specific Reynolds number. Despite extensive documentation on this classical flow, particularly at the mentioned Reynolds number associated with a subcritical flow regime, consensus regarding turbulence statistics just behind the obstacle remains lacking. The study employs both numerical simulations via large eddy simulation and experimental techniques such as hot-wire anemometry and particle image velocimetry. Numerical simulations utilize high-order schemes and an immersed boundary method. Emphasizing turbulence statistics and power spectra in the near wake up to ten diameters, the study highlights the challenges of statistical estimation, necessitating long integration times that increase computational costs and introduce uncertainties of approximately 10% for most flow characteristics. While numerical and experimental results align well with previous large eddy simulation data, discrepancies with experimental data from existing literature are observed, exceeding the estimated uncertainty range. Consequently, the research suggests a reduction in previous numerical-experimental controversies for this flow, presenting new data that contribute to resolving discrepancies.

Guo et al. (2019) address the challenges posed by the installation of pipelines in deep-sea areas, particularly where they traverse complex topographic conditions such as submarine canyons. The seabed in these regions is susceptible to erosion and shaping by active deep-sea currents, leading to variations in pipeline span heights. Furthermore, the occurrence of deep-sea geological hazards, including submarine landslides, poses a serious threat to pipeline safety. To mitigate these risks, the researchers develop an improved numerical analysis method integrating low-temperature rheological models of landslides and geometric model optimization. This approach enables the simulation of landslide impacts on pipelines. The study systematically investigates the influence of span heights on the forces exerted on pipelines by deep-sea landslides, proposing three modes of forces and related mechanisms. Additionally, they introduce the concept of span height ratio and establish four formulas to evaluate pipeline forces. Their analysis reveals significant increases in lift force coefficients, up to nearly 20 times, when considering different span heights. Overall, this research provides a theoretical framework for designing and protecting deep-sea pipelines against the impacts of geological hazards.

Dong et al. (2022) conducted simulations of submarines sailing near the free surface with long-crested waves using an in-house viscous URANS solver with an overset grid approach. The study began with verification and validation procedures to assess reliability, confirming accurate irregular wave generation and good agreement of total resistance results with experimental

fluid dynamics (EFD) data. Three different submerged depths ranging from 1.1D to 3.3D were selected to simulate submarine sailing near calm water, comparing the results to investigate the influence of irregular waves and submerged depths. The simulations revealed that the free surface leads to increased resistance, lift, and bow-up moments of the model, with this effect diminishing significantly at greater submerged depths. Irregular waves caused substantial fluctuations in hydrodynamic forces and moments, persisting even at deeper submerged depths, which could complicate submarine control strategies. The response spectrum of hydrodynamic forces and moments exhibited slight amplitudes in the high-frequency region, indicating less sensitivity of the model to high-frequency excitations.

Uzun et al. (2021) aimed to assess the impact of biofouling-related hull roughness on a full-scale submarine, focusing on resistance components, effective power, and nominal wakefield using Computational Fluid Dynamics. They initially validated the study with model-scale submarine data under hydraulically smooth conditions. Subsequently, they incorporated roughness functions representing various biofouling levels into a Reynolds-Averaged Navier-Stokes (RANS) solver's wall function. The study investigated the full-scale submarine under both smooth and different biofouling-related roughness conditions. Scale effects between model and full-scale submarines were examined based on total resistance components and nominal wake fraction under smooth conditions. In rough cases, frictional resistance values obtained by the RANS solver for the full-scale submarine were compared with predictions using Granville's similarity law analysis. Results showed a significant increase in effective power (ranging from ~36% to ~112%) with roughness height and submarine speed. Additionally, increasing boundary layer thickness due to roughness led to higher mean nominal wake fraction values (ranging from ~25% to ~68%) compared to reference values in the axial direction at the stern.

Airfoil simulations are essential for optimizing a submarine's control surfaces, such as rudders and dive planes, which function like aircraft wings to enhance maneuverability and stability. Using Computational Fluid Dynamics, researchers analyze lift, drag, and flow behavior to refine surface geometry, reducing resistance while maximizing control. These simulations improve turning, diving, and energy efficiency while enabling virtual testing before prototyping, saving time and costs. Ultimately, they enhance hydrodynamic performance for optimal underwater operation. Wu Xiaocui et al. (2015) developed a hybrid reference frame method combining rotating reference frames and added a momentum source method for maneuverability simulations. The approach uses a single mesh for various conditions, and validation showed stability derivatives for a yawing moment and force-matched experimental data with minimal errors. The study also analyzed the effects of rotating arm radius, pitch, and drift angles, proving the method's applicability to engineering designs. Zhang et al. (2025) investigated the motion stability of a rough submarine in the vertical plane near the seabed using numerical simulations, including oblique towing, pure

heave, and pitch tests. The study analyzed the effects of roughness height, distribution, and seabed distance, revealing that both hull roughness and proximity to the seabed significantly reduce stability, with an 85.75% decrease in extreme cases. Stern one-third hull fouling had the most detrimental effect, reducing stability by 57.83% compared to 17.04% and 10.00% for forward and middle one-third fouling, respectively. Minimizing stern fouling was identified as the most effective measure for improving stability. Dubbioso et al. (2017) analyzed the maneuvering characteristics of a submarine using an unsteady RANS-based CFD solver, comparing cruciform (C) and X-shaped rudder configurations in 3DoF horizontal maneuvers. The X rudder demonstrated superior turning performance, though it required forward plane deflection for depth control, while stern appendages acted as fixed surfaces during steady turning. Grid refinement analysis indicated that a coarse grid provided reliable trajectory predictions but required finer resolution for accurate hydrodynamic load estimation. Partial validation for the C rudder showed a steady turning diameter error of  $\sim 10\%$ , highlighting the potential of CFD for submarine maneuvering studies. Stevanović et al. (2016) compared two mechanical designs of a river submarine robot for delicate underwater tasks. Emphasizing reduced hydrodynamic drag and improved mobility, the new design adopts a streamlined, biomimetic form inspired by fast-swimming animals, optimizing the fineness ratio. Fluid dynamics simulations were used to evaluate performance. The study also simulated robot control using a mathematical model and a PID controller, analyzing trajectory tracking under river flow disturbances. Wang et al. (2015) investigated a 4000 TEU containership without considering free surface effects. They numerically resolved the viscous flow fields of the ship at different scales using the Reynolds-Averaged Navier-Stokes (RANS) method. Additionally, they employed numerical uncertainty analysis based on the factors of safety method for Richardson extrapolation. The study focused on analyzing the scale effect of the axial nominal wakefield in detail. Their findings revealed that the reciprocal of the mean axial wake fraction of the propeller disc exhibited a near-linear dependence on the Reynolds number on the logarithmic scale. For a single-screw ship without bilge vortex, a linear function fits perfectly for the relationship between the reciprocal of mean axial wake fraction at each radius, the reciprocal of the amplitude of wake peak right above the propeller disc, and Reynolds number in logarithmic scales. In the inner area of the propeller disc, the reciprocal amplitude of the wake valley and wake peak right down the propeller disc showed a nearly linear dependence on the Reynolds number in logarithmic scales. However, in the outer area, the amplitude of the wake peak and valley declined rapidly to the potential wake fraction, and the wake width revealed a negative exponent power function dependence on the Reynolds number in logarithmic scales. Building on these insights, the authors proposed an extrapolated wake field scaling method. The aim of this research article is to investigate the flow dynamics of submarines at high angles of attack on the vertical plane. The main aim of this research article is to

improve the knowledge and understanding of underwater submarine hydrodynamics and provide a comprehensive description of the implementation of optimization techniques using adjoint functions, enabling intelligent and automatic shape optimization with minimal turnaround time for numerical computations

## 2. NUMERICAL MODEL

### 2.1 Geometry

The paper's simulations predominantly focused on solving the incompressible Reynolds Averaged Navier-Stokes (RANS) equations utilizing the segregated flow solver within the commercial CFD code Ansys. To ensure efficient evaluation of concept designs on a regular basis, it is imperative to manage the time required for preparing a computational model from CAD geometry and executing and analyzing a standard series of tests within reasonable constraints. Consequently, significant efforts have been devoted to automating these processes, facilitated by Ansys' extensive accessibility to its underlying functionality through an adjoint solver rather than a proprietary scripting language. This automation extends to generating and meshing appropriate computational domains for various tests based on model geometry and test specifications, as shown in Figure 1.

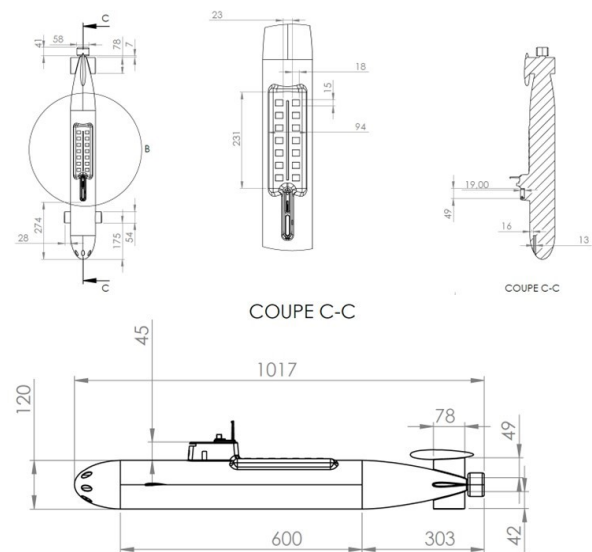


**Figure 1. The submarine has dimensions of 48.8 meters in length and a midsection diameter of approximately 6 meters, expanded for enhanced reliability.**

All tests utilized an unstructured hexahedral mesh with a prism layer adjacent to solid surfaces. Mesh refinement was selectively applied in the vicinity of the submarine and downstream where the wake forms, guided by scaling rules derived from practical experience. The prism layer consisted of sub-layers increasing in thickness away from the wall in a geometric progression. The expansion factor typically ranges from 1 to 2 or less. Turbulence model wall treatments impose constraints on the thickness of the sub-layer closest to the wall. For example, low-Re turbulence models necessitate a  $y^+$  value around 27.6 for coarse mesh and approximately 29 for fine mesh at the centroid of the

layer, where  $y^+$  represents a non-dimensional distance perpendicular to the wall. Alternatively, when employing a wall function, the centroid of the first layer should lie within the law of the wall region. To define a prism layer meeting these criteria, the hull's length ( $L_{oA}$ ) or half-span chord for fins and control surfaces can be used as a reference.

The flat boundary layer can be expressed by the following equation [1]:

$$2 \left( \frac{uy^+}{yU} \right)^2 = \frac{0.455}{\ln^2(0.06 \text{Re} x)} \quad (1)$$

The boundary layer thickness,  $\delta$ , is estimated using the following equation:

$$\frac{\delta}{x} \approx \frac{0.16}{(\text{Re} x)^{1/7}} \quad (2)$$

## 2.2 Mesh generation

In a static incidence test, a model is towed at various angles of incidence relative to the towing direction. To replicate this test in software, we have opted to keep the submarine model fixed within a rectangular domain while adjusting the flow direction. In Figure 2, the upstream boundary and the port and starboard boundaries are designated as inlet boundaries, with the appropriate flow direction and magnitude specified. The downstream boundary is set as a pressure boundary, while the top and bottom boundaries are defined as slip walls. This approach offers the advantage of allowing for domain re-meshing to enhance refinement in the wake direction across a series of tests covering different drift angles. Additionally, the solution converged from the previous test is interpolated onto the new mesh to establish an initial flow for the subsequent iteration. The base case with the coarse mesh comprises approximately 3.1 million cells, while the fine mesh consists of approximately 6.275 million cells.

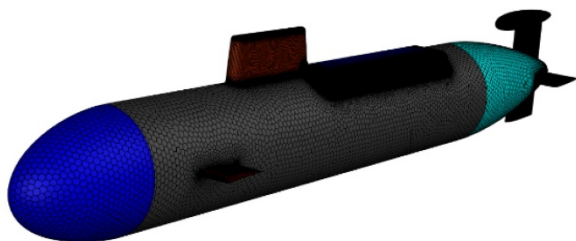


Figure 2. A refinement mesh has been applied to the model

## 2.3 Boundary conditions and grid

In the subsequent analysis, test data for the submarine equipped with a fin configuration are examined. For the submarine with control surfaces, specific symmetries in the configurations lead to several maneuvering coefficients effectively approaching zero. This absence of test data in the literature pertains particularly to the fully appended configuration. Simulations were conducted utilizing a prism layer generated to achieve a target wall  $y^+$  of 0.8. The turbulence models employed in these simulations include:

- Spalart and Allmaras (SA)
- SST
- Wilcox k-omega (k- $\omega$ )
- k-epsilon (k- $\epsilon$ ) model with low Reynolds number wall treatment

The drag coefficient ( $C_{xa}$ ) and lift coefficient ( $C_{ya}$ ) at various angles of attack are presented in Table 1, obtained using a coarse mesh, and in Table 2 for the fine mesh.

Table 1. The drag coefficient and lift coefficient for different angles of attack using a coarse mesh

Coarse mesh		
AoA	$C_{xa}$	$C_{ya}$
20	0.295884	0.834301
80	2.856846	0.845926

Table 2. The drag coefficient and lift coefficient for different angles of attack using a fine mesh

Fine mesh		
AoA	$C_{xa}$	$C_{ya}$
20	0.305795	0.825117
80	2.804608	0.817119

## 2.4 Governing equations

In submarine operations, particularly at low speeds, the compressibility of water can be disregarded, allowing the flow to be treated as incompressible. In such cases, the Navier-Stokes equations are employed to describe the flow, as demonstrated below [11-15]:

Navier-Stokes Equations:

$$\nabla \cdot \mathbf{v} = 0 \quad (3)$$

$\rho$  represents the density of the fluid (water),  $\mathbf{v}$  is the velocity vector,  $p$  stands for pressure,  $\mu$  is the dynamic viscosity, and  $\mathbf{g}$  denotes the gravitational acceleration vector.

Continuity Equation:

$$\rho \left( \frac{\partial \mathbf{v}}{\partial t} + \mathbf{v} \cdot \nabla \mathbf{v} \right) = -\nabla p + \mu \nabla^2 \mathbf{v} + \rho \mathbf{g} \quad (4)$$

## 3. RESULTS AND DISCUSSIONS

### Pressure coefficient of base model for different the angle of attack (AoA)

Figure 3(a) shows that at an AoA of  $\theta = 20^\circ$ , the coarse mesh reveals a high-pressure coefficient at the front of the submarine, with lower values on the wings attached to the middle and rear sections. This observation aligns with Figure 3(b), where the fine mesh results corroborate the pressure distribution seen in the coarse mesh, indicating consistency in the data. At a higher AoA of  $\theta = 80^\circ$ , Figure 3(c) demonstrates that the coarse mesh shows only slight pressure at the front and bottom of the submarine, with the most significant loads occurring at the upper part and wings. These findings are confirmed by Figure 3(d), where the fine mesh results mirror those of the coarse mesh, further validating the accuracy of the pressure coefficient measurements across different mesh densities. This consistency across mesh types underscores the effectiveness

of the optimization techniques employed in assessing the submarine's hydrodynamic performance under varying angles of attack.

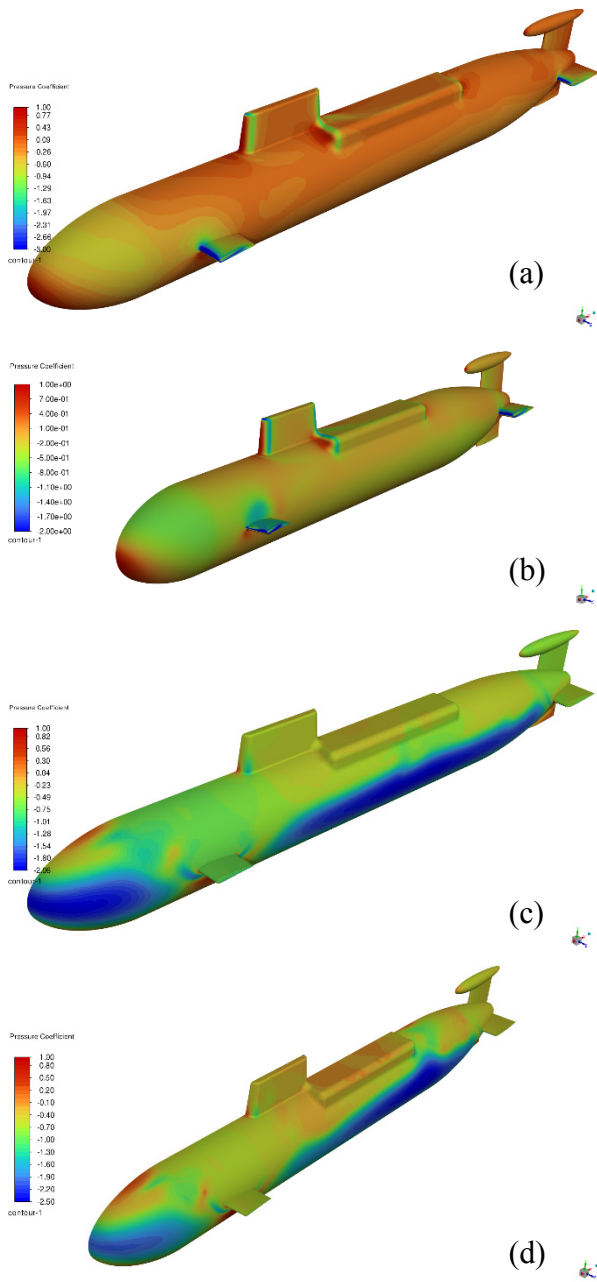


**Figure 3** (a) Pressure coefficient for coarse mesh at the impact of the angle of attack of  $\theta=20^\circ$ , (b) Pressure coefficient for fine mesh at the impact of the angle of attack of  $\theta=20^\circ$ , (c) Pressure coefficient for coarse mesh at the impact of the angle of attack of  $\theta=80^\circ$ , (d) Pressure coefficient for fine mesh at the impact of the angle of attack of  $\theta=80^\circ$

**Velocity contour of AoA = 20°**

Figure 4 presents the velocity contours around an airfoil at an angle of attack (AoA) of 20°, comparing the velocity distribution for coarse and fine mesh at different plane sections. Figure (a) illustrates the velocity distribution in the front plane section for a coarse mesh, showing a general representation of the flow field, particularly in the high-velocity region on the upper surface of the airfoil.

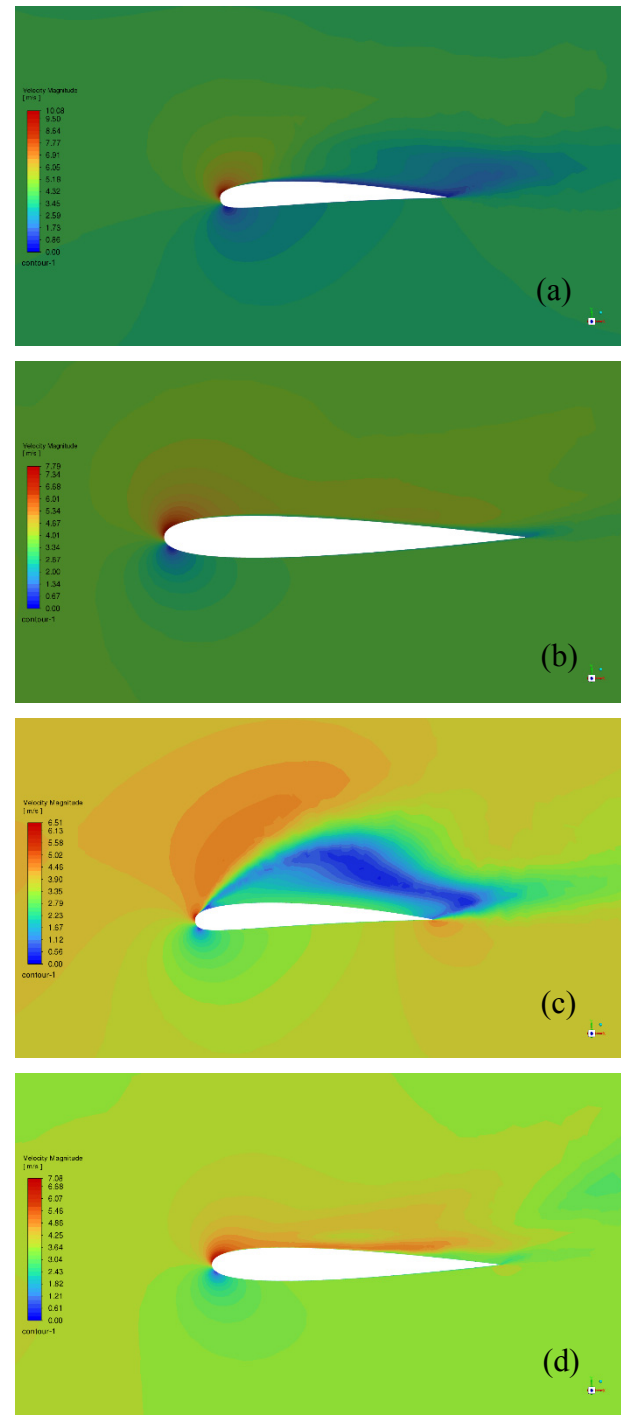


**Figure 4.**Velocity contour of AoA =20° (a) Velocity distribution in the front plane section for coarse mesh, (b) Velocity distribution in the rear plane section for coarse mesh, (c) Velocity distribution in the front plane section for fine mesh, (d) Velocity distribution in the rear plane section for fine mesh

Similarly, Figure (b) depicts the velocity distribution in the rear plane section for a coarse mesh, capturing the overall flow behavior, including the wake, but with reduced clarity in the flow gradients and fine structures. In contrast, Figure (c) shows the velocity distribution in the front plane section for a fine mesh, providing a more detailed and accurate depiction of the high-velocity region on the upper surface and the low-velocity zone near the stagnation point. Finally, Figure (d) presents the velocity distribution in the rear plane section for a fine mesh, offering a clearer representation of the

velocity gradients and wake behavior. The comparison demonstrates the superior accuracy and detail achieved with a fine mesh, which is essential for analyzing complex flow phenomena and aerodynamic performance at higher angles of attack.

### Velocity contour of AoA = 80°

Figure 5 illustrates the velocity contour of an airfoil at an angle of attack 80° for both coarse and fine mesh configurations, comparing the velocity distributions in the front and rear plane sections. Figure 5(a) depicts the velocity distribution in the front plane section using a coarse mesh, showing a region of high velocity near the leading edge on the upper surface due to flow acceleration, while the lower surface experiences slower flow.

Figure 5(b) presents the velocity distribution in the rear plane section with a coarse mesh, where the flow separation at the trailing edge results in an uneven velocity gradient, highlighting the limitations of the coarse resolution. In Figure 5(c), the fine mesh provides a detailed representation of the velocity distribution in the front plane section, with smoother contours and better capture of sharp transitions. Figure 5(d) illustrates the rear plane section for the fine mesh, where flow separation and low-velocity zones at the trailing edge are resolved more accurately, revealing critical flow features such as eddies. The comparison emphasizes that the fine mesh enhances the accuracy of flow resolution, particularly in capturing complex flow phenomena at high angles of attack.

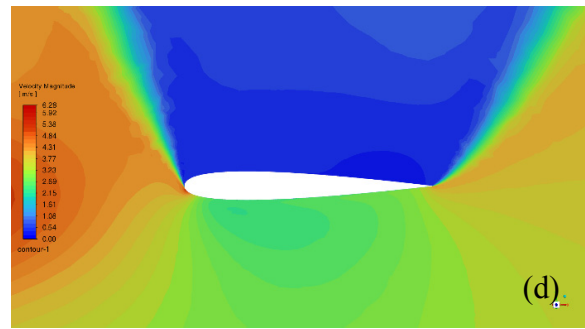
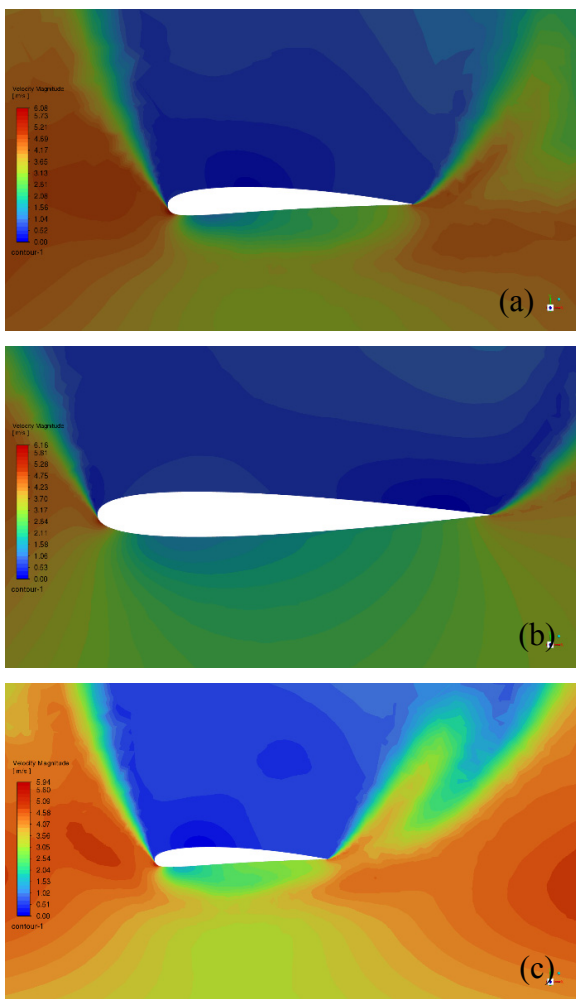
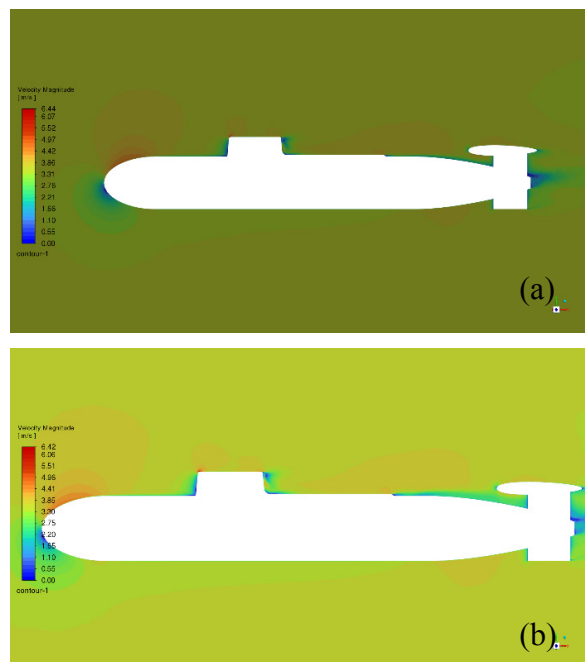
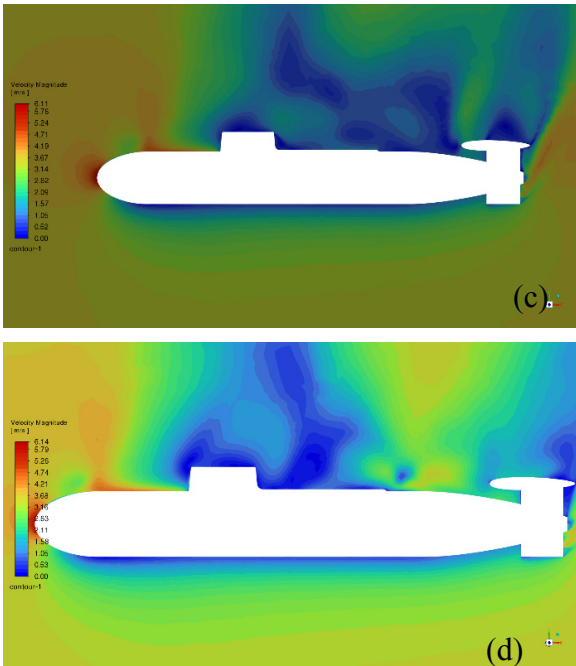


Figure 5 Velocity contour of AoA = 80° (a) Velocity distribution in the front plane section for coarse mesh, (b) Velocity distribution in the rear plane section for coarse mesh, (c) Velocity distribution in the front plane section for fine mesh, (d) Velocity distribution in the rear plane section for fine mesh

### 3.4 Velocity distribution in symmetry section of different AoA

The examination of velocity distribution at angles of attack (AoA) of 20° and 80° is presented in Figure 6. Figure 6(a) shows the velocity distribution in the symmetry section for a coarse mesh at an AoA of 20°, where the recorded velocity values are within an acceptable range, indicating a stable flow around the submarine. This result is consistent with Figure 6(b), where the fine mesh at the same AoA also exhibits a similar velocity distribution, confirming the reliability of the coarse mesh analysis. At a higher AoA of 80°, Figure 6(c) demonstrates the velocity distribution for the coarse mesh, where some areas of stagnant flow appear on the upper part of the submarine body, suggesting a potential flow separation. This observation is further supported by Figure 6(d), where the fine mesh reveals a similar pattern of velocity distribution at an AoA of 80°, emphasizing the challenges in maintaining flow stability at higher angles of attack. These findings highlight the differences in flow behavior at varying AoAs and the importance of mesh resolution in capturing the details of fluid dynamics around the submarine.





**Figure 6** (a) Velocity distribution in symmetry section for a coarse mesh of AoA = 20°, (b) Velocity distribution in symmetry section for a fine mesh of AoA = 20°, (c) Velocity distribution in symmetry section for a coarse mesh of AoA = 80°, (d) Velocity distribution in symmetry section for a fine mesh of AoA = 80°

### 3.5 Adjoint optimization function

The adjoint optimization function in ANSYS software proposed a new design aimed at enhancing performance concerning different angles of attack (AoA). This was achieved by modifying the design parameters of the wings and the submarine's entire body to suit various conditions better, as illustrated in Figure 7 and detailed in Table 3.

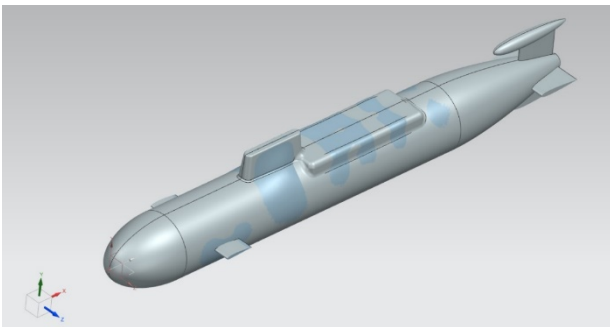


**Figure 7** ISOVIEW generated from the Adjoint optimization function

**Table 3** The drag coefficient and lift coefficient for angles of attack  $\theta = 0^\circ$  for both base and optimal cases

Parameter	Base	Optimal
AoA	Cx0	Cy0
0	0.059586	0.048021

### 3.5.1 Pressure coefficient of optimal design

The pressure coefficient for the optimal design, shown in Figure 8 for a fine mesh at an angle of attack (AoA) of 0°, indicates an evenly distributed pressure load across the surface.

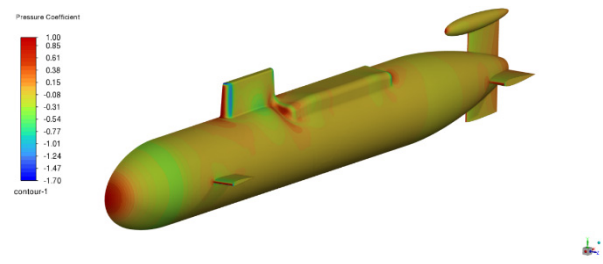


**Figure 8.** Pressure coefficient of optimal design for fine mesh at the impact of AoA = 0°

### 3.5.2 Velocity contour of the optimal design

Figure 9 presents the velocity contour of an airfoil at an angle of attack of 0°, showcasing the velocity distributions in both the front and rear plane sections using a fine mesh in an optimized design. In Figure 9(a), the velocity distribution in the front plane section is illustrated. The flow field around the airfoil exhibits symmetry due to the zero angle of attack. The velocity increases smoothly over the upper and lower surfaces near the leading edge, with no significant regions of separation or turbulence. This indicates efficient flow attachment along the airfoil. In Figure 9(b), the velocity distribution in the rear plane section is displayed. The contours show the continuation of the smooth flow over the trailing edge, with a gradual reduction in velocity as the flow exits the airfoil. The absence of significant low-velocity zones or separation regions further demonstrates that the optimized design achieves effective aerodynamic performance at this angle of attack. The comparison between the front and rear plane sections highlights the streamlined flow behavior and uniform velocity distribution around the airfoil, facilitated by the use of a fine mesh in the optimal design. This ensures accurate resolution of flow features, essential for evaluating the aerodynamic performance at 0°.

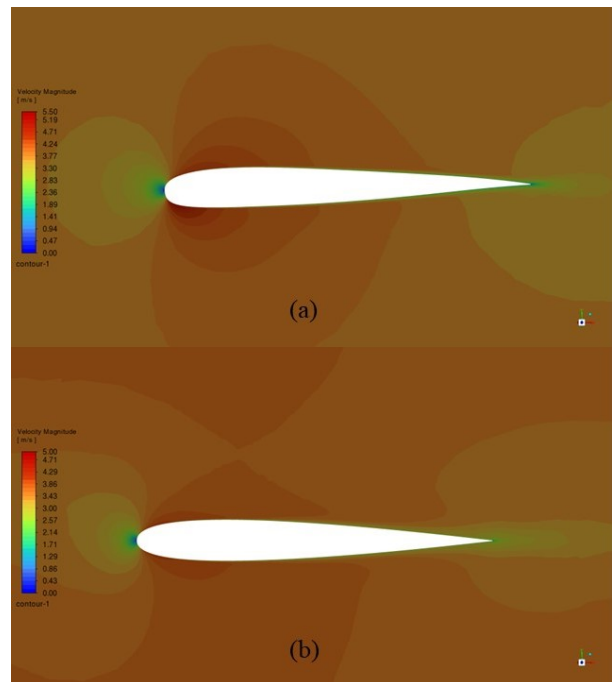


**Figure 9** Velocity contour of AoA = 0° (a) Velocity distribution in optimal design front plane section for fine mesh, (b) Velocity distribution in the rear plane section for fine mesh

### 3.5.3 Velocity distribution in the symmetry section of optimal design

Figure 10 depicts the velocity distribution in the symmetry section for a fine mesh at an angle of attack (AoA) of  $0^\circ$ . The maximum recorded velocity is 6 m/s, with a minimal stagnant state observed at the rear part of the submarine.

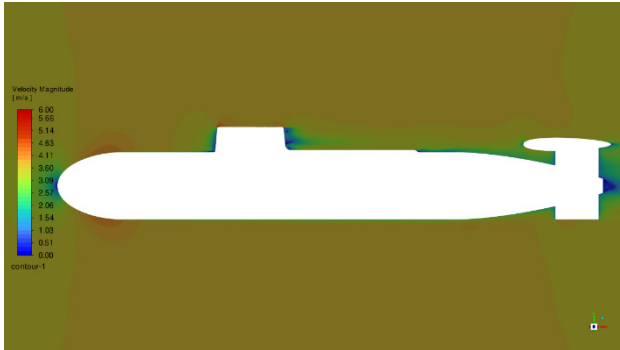


**Figure 10** Velocity distribution in symmetry section for a fine mesh of AoA =  $0^\circ$

## 4. CONCLUSIONS

The study underscores the effectiveness of computational fluid dynamics (CFD) simulations in evaluating and optimizing hydrodynamic and aerodynamic performance. By leveraging the incompressible Reynolds Averaged Navier-Stokes (RANS) equations and utilizing advanced features of ANSYS software, the research highlights the importance of fine mesh resolution in accurately capturing flow behaviors across varying angles of attack. The comparative analysis between coarse and fine meshes consistently demonstrates that finer meshes provide superior detail, particularly in resolving critical flow phenomena such as velocity gradients, wake behavior, and pressure distributions. The integration of automation in generating and meshing computational domains further enhances the efficiency of simulation workflows, allowing for iterative design improvements. The investigation of submarines equipped with control surfaces revealed unique flow symmetries and identified maneuvering coefficients that approach zero due to the configurations. Notably, the adjoint optimization function within ANSYS enabled the development of an improved design, resulting in enhanced aerodynamic performance, as evidenced by reduced drag and improved flow stability at different angles of attack. The findings emphasize the value of adopting precise simulation techniques and optimization algorithms to address complex engineering challenges. These advancements not only streamline design processes but also contribute to the development of high-performance marine and aerodynamic structures, paving the way for more efficient and innovative designs in future applications.

## REFERENCES

- [1] Marshallsay, P. G., and Eriksson, A. M., "Use of Computational Fluid Dynamics as a Tool to Assess the Hydrodynamic Performance of a Submarine," Proc. 18th Australasian Fluid Mech. Conf., Launceston, Australia, 2012.
- [2] Mozaffari, S., Guilmineau, E., Visonneau, M., and Wackers, J., "Average-Based Mesh Adaptation for Hybrid RANS/LES Simulation of Complex Flows," *Computers & Fluids*, 232, p. 105202, 2022.
- [3] Parnaudeau, P., Carlier, J., Heitz, D., and Lamballais, E., "Experimental and Numerical Studies of the Flow Over a Circular Cylinder at Reynolds Number 3900," *Phys. Fluids*, 20(8), p. 085101, 2008.
- [4] Guo, X.-S., Zheng, D.-F., Nian, T.-K., and Yin, P., "Effect of Different Span Heights on the Pipeline Impact Forces Induced by Deep-Sea Landslides," *Appl. Ocean Res.*, 87, pp. 38-46, 2019.
- [5] Dong, K., Wang, X., Zhang, D., Liu, L., and Feng, D., "CFD Research on the Hydrodynamic Performance of Submarine Sailing Near the Free Surface With Long-Crested Waves," *J. Mar. Sci. Eng.*, 10(1), p. 90, 2022.
- [6] Uzun, D., Sezen, S., Ozyurt, R., Atlar, M., Turan, O., "A CFD Study: Influence of Biofouling on a Full-Scale Submarine," *Appl. Ocean Res.*, 109, p. 102561, 2021.
- [7] Wu, X., Wang, Y., Huang, C., Hu, Z., Yi, R., "An effective CFD approach for marine-vehicle maneuvering simulation based on the hybrid reference frames method," *Ocean Engineering*, 109, 83-92, 2015.
- [8] Zhang, X., Huo, J., Zhang, M., Cai, X., Wang, B., Xie, Z., "Maneuverability characteristics of a fouling submarine near the seabed," *Ocean Engineering*, vol. 315, p. 119773, 2025.
- [9] Dubbioso, G., R. Broglia, S. Zaghi. "CFD Analysis of Turning Abilities of a Submarine Model." *Ocean Engineering* 129: 459-79, 2017.
- [10] Stevanović, I., Ćosić, A., Rodić, A., Rašuo, B., "Biologically Inspired Design and Hydrodynamic Analysis of a Remotely Operated Vehicle for River Underwater Tasks," *International Journal of Mechanics and Control*, Vol. 17, No. 01, pp. 13-21, 2016.
- [11] Wang, Z.-Z., Xiong, Y., Wang, R., Shen, X.-R., and Zhong, C.-H., "Numerical Study on Scale Effect of Nominal Wake of Single Screw Ship," *Ocean Eng.*, 104, pp. 437-451, 2015.
- [12] Vali, A., Saranjam, B., Kamali, R., "Experimental and Numerical Study of a Submarine and Propeller Behaviors in Submergence and Surface Conditions," *J. Appl. Fluid Mech.*, 11(5), pp. 1297-1308, 2018.
- [13] Bakica, A., Vladimir, N., Jasak, H., Kim, E. S., "Numerical Simulations of Hydrodynamic Loads and Structural Responses of a Pre-Swirl Stator," *Int. J. Nav. Archit. Ocean Eng.*, 13, pp. 804-816, 2021.
- [14] Rostamzadeh-Renani, M., Rostamzadeh-Renani, R., Baghoolizadeh, M. Khabazian Azarkhavarani, N., "The effect of vortex generators on the hydrodynamic performance of a submarine at a high

angle of attack using a multi-objective optimization and computational fluid dynamics,” *Ocean Engineering*, 282, p.114932, 2023.

- [15] Polishchuk, M., Rolik, O., “Improvement of Technological Equipment Drone for Water Sampling: Design and Modeling,” *FME Transactions*, vol. 52, no. 2, pp. 237–245, 2024.

---

## МЕТОДОЛОГИЈА ОПТИМИЗАЦИЈЕ ДИЗАЈНА ПОДМОРНИЦЕ КОРИШЋЕЊЕМ ВИШЕСЛОЈНИХ НУМЕРИЧКИХ ЦФД МОДЕЛА

**Б. Мохамад, С. Амрун, Р. Мири,  
А. Беншекур, К. Галојан**

Ова студија истражује хидродинамичке и аеродинамичке перформансе подморнице и аеропрофила под различитим угловима напада (AoA) користећи напредне симулације рачунарске динамике флуида (ЦФД). Нестишљиве Реинолдсове просечне Навиер-Стокес (РАНС) једначине су решене коришћењем АНСИС-а, користећи његов одвојени решавач тока и могућности адјоинт оптимизације за аутома-

тизацију креирања и умрежавања рачунарских домена. Анализом расподеле брзине и притиска у резолуцијама грубих и финих мрежа, истраживање наглашава супериорну тачност финих мрежа у хватању сложених феномена протока, као што су одвајање протока, понашање у буђењу и градијенти брзине. Симулације подморница са контролним површинама откриле су различите симетрије и скоро нулте коефицијенте маневрисања за специфичне конфигурације, попуњавајући празнине у постојећој литератури о потпуно доданим геометријама. Напори на оптимизацији довели су до побољшаног дизајна са побољшаном аеродинамичком ефикасношћу, постизањем смањеног отпора и стабилизованог протока, што је потврђено доследним перформансама при AoA од 0°, 20° и 80°. Овај рад показује важност резолуције fine мреже, аутоматизованих радних токова и повезаних решавача у убрзавању итеративног процеса пројектовања и оптимизацији поморских и аеродинамичких структура за примене у стварном свету. Ови налази наглашавају значајан утицај великих углова напада на вертикални ток подморнице. Такви увиди нуде механичку основу за анализу феномена нелинеарног кретања током изрона подморнице.